Molecular Changes following Oxidoreduction of Cytochrome *b*559 Characterized by Fourier Transform Infrared Difference Spectroscopy and Electron Paramagnetic Resonance: Photooxidation in Photosystem II and Electrochemistry of Isolated Cytochrome *b*559 and Iron Protoporphyrin IX–Bisimidazole Model Compounds†

Catherine Berthomieu,*,‡ Alain Boussac,‡,§ Werner Mäntele,‖ Jacques Breton,‡ and Eliane Nabedryk‡

Section de Bioénergétique, Département de Biologie Cellulaire et Moléculaire, Centre d'Etudes Nucléaires de Saclay, 91191 Gif-sur-Yvette Cedex, France, and Institut für Biophysik und Strahlenbiologie, Universität Freiburg, Albertstrasse 23, 7800 Freiburg, Germany

Received July 7, 1992; Revised Manuscript Received August 28, 1992

ABSTRACT: The vibrational infrared absorption changes associated with the oxidation of cytochrome *b*559 (Cyt *b*559) have been characterized. In photosystem II (PS II) enriched membranes, low-potential (LP) and high-potential (HP) Cyt *b*559 were investigated by light-induced FTIR difference spectroscopy. The redox transition of isolated Cyt *b*559 is characterized by protein electrochemistry. On the basis of a model of the assembly of Cyt *b*559 with the two axial Fe ligands being histidine residues of two distinct polypeptides, each forming a transmembrane α-helix [Cramer, W. A., Theg, S. M., & Widger, W. R. (1986) *Photosynth. Res. 10,* 393–403], the bisimidazole and bismethylimidazole complexes of Fe protoporphyrin IX were electrochemically oxidized and reduced to detect the IR oxidation markers of the heme and its two axial ligands. Major bands at 1674/1553, 1535, and 1240 cm^{-1} are tentatively assigned to ν37(CaCm), ν38-(CbCb) and δ(CmH) modes, respectively; other bands at 1626, 1613, 1455, 1415, and 1337 cm^{-1} are assigned to porphyrin skeletal and vinyl modes. Modes at 1103 and 1075/1066 cm^{-1} are assigned to the 4-methylimidazole and imidazole ligands, respectively. For the isolated Cyt *b*559, it is shown that both the heme (at 1556–1535, 1337, and 1239 cm^{-1}), the histidine ligands at 1104 cm^{-1} and the protein (between 1600 and 1700 cm^{-1} and at 1545 cm^{-1}) are affected by the charge stabilization. The excellent agreement between model compounds and isolated Cyt *b*559 reinforces the validity of the model of a heme iron coordinated to two histidine residues for Cyt *b*559. A differential signal at 1656/1641 cm^{-1} is assigned to peptide C=O mode(s). We speculate that this signal reflects the change in strength of a hydrogen bond formed between the histidine ligand(s) and the polypeptide backbone upon oxidoreduction of the cytochrome. In PS II membranes, the signals characteristic of Cyt *b*559 photooxidation are found at 1660/1652 and 1625 cm^{-1}, for both the high- and low-potential forms. The differences observed in the amplitude of the 1660/1652-cm^{-1} band, at 1700 and 1530–1510 cm^{-1} in the light-induced FTIR difference spectra of Cyt *b*559 HP and LP, show that the mechanisms of heme oxidation in vivo imply different molecular processes for the two forms Cyt *b*559 HP and LP.

Photosystem II (PS II)[1] of plants and cyanobacteria is a membrane complex that converts the energy of a photon in a charge-separated state between a (chlorophyllic) primary electron donor, P_{680}, and an intermediary electron acceptor, pheophytin. The energy is further stabilized by migration of the electron on two plastoquinones, Q_A and then Q_B. The oxidized primary donor P_{680}^+ is reduced via a tyrosine residue by the oxygen-evolving complex (OEC), a complex able to extract electrons from water [see Rutherford et al. (1992) for a review]. The reaction center (RC) of PS II presents functional and structural analogies to the photosynthetic RC of purple photosynthetic bacteria, whose three-dimensional structure has been elucidated (Allen et al., 1987; Deisenhofer et al., 1985; El-Kabbani et al., 1991). In the bacterial RC, two polypeptides L and M constitute the anchoring site of the redox carriers involved in the first events of charge separation and electron stabilization and are assembled with a third polypeptide, H. For PS II, the smallest purified RC unit, D_1D_2Cyt *b*559 particle (Namba & Satoh, 1987), contains two polypeptides, D_1 and D_2, analogous to L and M, respectively, associated with cytochrome *b*559 (Cyt *b*559), a membranous *b*-type cytochrome. The direct implication of Cyt *b*559 in the first events of charge separation has not been demonstrated under physiological conditions, but its ability to rereduce or reoxidize redox carriers involved in the primary photosynthetic processes has been observed. At low temperature, Cyt *b*559 acts as an electron donor to P_{680}^+ (Knaff & Arnon, 1969; Verméglio & Mathis, 1974), being an alternative or a secondary donor to a chlorophyll (Chl) molecule (dePaula et al., 1985; Visser & Rijgersberg, 1975). Furthermore, its

† Part of this work was supported by the PROCOPE program and the European Communities (SC1000335). W.M. gratefully acknowledges a Heisenberg fellowship from the Deutsche Forschungsgemeinschaft.

* To whom correspondence should be addressed. Present address: Max-Planck-Institut für Biophysik, Heinrich Hoffmann-Str. 7, 6000 Frankfurt/Main 71, FRG.

‡ CEN Saclay.

§ Supported by the CNRS (URA 1290).

‖ Universität Freiburg.

[1] Abbreviations: PS II, photosystem II; BBY, photosystem II-enriched membranes; OEC, oxygen-evolving complex; RC, reaction center; Q_A (Q_B), primary (secondary) electron acceptor plastoquinone; Cyt *b*559, cytochrome *b*559; Chl, chlorophyll; P_{680}, primary electron donor; FTIR, Fourier transform infrared; EPR, electron paramagnetic resonance; RR, resonance Raman; Tris, tris(hydroxymethyl)aminomethane; Mes, 2-(*N*-morpholino)ethanesulfonic acid; PATs-4, pyridine-4-carboxaldehyde thiosemicarbazone; Im, imidazole; 4-MeIm, 4(5)-methylimidazole; 1-MeIm, 1-methylimidazole; PP, protoporphyrin IX; TPP, tetraphenylporphyrin; OEP, octaethylporphyrin; CTABr, cetyltrimethylethylammonium bromide; HP, high potential; LP, low potential; SHE, standard hydrogen electrode; SCE, saturated calomel electrode.

0006-2960/92/0431-11460$03.00/0 © 1992 American Chemical Society

reduction by quinone analogues in D_1D_2Cyt *b*559 complexes has been demonstrated (Satoh et al., 1990), and a role in a cyclic electron transfer around PS II proposed from different experiments (Arnon & Tang, 1988; Heber et al., 1979; Thompson & Brudwig, 1988). The role of this cyclic electron transfer would be a protection against photoinhibition—the irreversible oxidation of chlorophyll or amino acid molecules due to the unusually high midpoint potential of P_{680}^+/P_{680} (1.17 V; Klimov et al., 1980) compared to the primary donor of all other photosynthetic RCs.

There is limited information concerning the organization of this cytochrome unit, which is absent in the RC of purple photosynthetic bacteria. The number of heme groups per P_{680} is probably one (Gounaris et al., 1989; Namba & Satoh, 1987; Widger et al., 1984) although the value of two has also been proposed (Dekker et al., 1989). A characteristic property of Cyt *b*559 is that is may exhibit different midpoint potentials (Rich & Bendall, 1980), depending on isolation and preparation conditions. In intact PS II membranes, most of the Cyt *b*559 is in a high-potential form with $E_m \approx 370$ mV (Cramer & Whitmarsh, 1977), i.e., extremely high compared to other *b*-type cytochromes (−200 to +120 mV) (Lemberg & Barrett, 1973). This high-potential (HP) form is readily altered to an intermediate- (IP) or low-potential (LP) form at high pH or by removal of the extrinsic proteins of the OEC by salt or Tris washing [reviewed in Thompson et al. (1989)]. Cyt *b*559 LP has a midpoint potential between 80 and 60 mV (Cramer & Whitmarsh, 1977). The midpoint potential of Cyt *b*559 LP has been reported as being pH dependent below pH 7.6 (Ortega et al., 1988).

The structure of Cyt *b*559 and the mechanisms involved in the conversion from the HP to LP forms are unknown. A model has been presented by Cramer et al. (1986) after the determination of the sequence of 27 N-terminal amino acids from the isolated cytochrome (Widger et al., 1984) that led to the sequencing of two neighboring genes located on the chloroplastic chromosome (Herrmann et al., 1984; Westhoff et al., 1985) and encoding for two polypeptides, subunits α and β. Each polypeptide, which contains a single histidine residue, is proposed to form a transmembrane α-helix. The apocytochrome would consist of a heterooligomeric $\alpha\beta$ structure (Widger et al., 1985). EPR and resonance Raman (RR) studies on the isolated Cyt *b*559 supported the model of a six-coordinated low-spin heme iron, with the fifth and sixth ligands being most probably two histidine residues (Babcock et al., 1985). These data led to the conclusion that the heme cross-links the histidine residues belonging to the two different polypeptides α and β. In this model, the heme is perpendicular to the membrane plane as previously inferred from spectroscopic measurements (Rutherford, 1985; Vermeglio et al., 1980). A change in the orientation of the imidazole plane of one of the histidine ligands was the only structural difference proposed to explain the different values of g_z observed by EPR spectroscopy for Cyt *b*559 HP and LP, with two perpendicular axial ligands in the Cyt *b*559 HP form (Babcock et al., 1985). Nevertheless, the effect of a rotation from parallel to perpendicular orientation of the axial ligands on the E_m values of the Fe^{III}/Fe^{II} couple was estimated to be of 50 mV (Walker et al., 1986), an effect too small to account for the difference of ≈300 mV observed between Cyt *b*559 HP and LP. Many other factors are known to influence the midpoint potential of cytochromes. Among them, the effect of the polarity of the heme environment (Churg & Warshel, 1986; Kassner, 1972) and the involvement of electrostatic interactions of the heme iron with charges buried around the heme or the propionic residues (Gunner & Honig, 1991; Moore et al., 1984) have been studied, as well as the interactions formed between the axial ligands and the protein (Valentine et al., 1979).

To gain further insight into the heme–protein interactions occurring in Cyt *b*559 and into the molecular mechanisms of Cyt *b*559 oxidation, we have used light-induced FTIR difference spectroscopy to study the photooxidation at low temperature of Cyt *b*559 HP and LP forms in PS II-enriched membranes. In addition, we have studied the redox transitions of the isolated Cyt *b*559 with electrochemically induced FTIR difference spectroscopy in vitro. With FTIR difference spectroscopy, information at a molecular level can be obtained (Braiman & Rothschild, 1988) and the nonselectivity of the IR absorption allows detection of signals arising from the heme and the protein. No information on the IR modes of heme groups sensitive to the oxidation state of the iron is available in the literature. In order to discriminate between the redox-sensitive modes of the protein and of the heme in Cyt *b*559, we studied the six-coordinated low-spin bisimidazole (Im) and bismethylimidazole (MeIm) complexes of iron protoporphyrin IX [$FePP(Im)_2$ and $FePP(MeIm)_2$] as model compounds simulating the coordination properties of the Cyt *b*559 heme. In each case, EPR controls have also been performed. The knowledge of the IR modes of these complexes is useful for the investigation of spectral data of a broad range of *b*-type cytochromes and heme proteins.

EXPERIMENTAL PROCEDURES

Model Compounds. The bis(1-methylimidazole) (1-MeIm) and bis[4(5)-methylimidazole] (4-MeIm) complexes of iron protoporphyrin, $FePP(1\text{-}MeIm)_2$ and $FePP(4\text{-}MeIm)_2$, respectively, were obtained by dissolution of 2.5 mM hemin chloride (purchased from Sigma and used without further purification) in a 50 mM phosphate buffer, pH 8, in the presence of 2% cetyltrimethylethylammonium bromide (CTABr), 100 mM KCl, and 1 M 1-MeIm or 4-MeIm (at pH 8), a procedure comparable to the one described in Desbois et al. (1989). For $FePP(4\text{-}MeIm)_2$, experiments were also performed at pD 12 and in D_2O (at pD 8). For bisimidazole (Im) or ^{15}N-labeled imidazole (^{15}NIm; 98% ^{15}N-labeled imidazole purchased from Euriso Top France) complexes with FePP, 5–7 mM hemin chloride was dissolved in a 50 mM phosphate buffer, pH 8, in the presence of 100 mM KCl, 15% CTABr, and 2 M Im or ^{15}NIm. The concentration of CTABr had to be as high as 15% in order to avoid aggregation effects at this hemin concentration. Nevertheless, the latter detergent concentration was also tested with the $FePP(4\text{-}MeIm)_2$ complex without any effect on the spectra.

Purification Procedure of Spinach Cytochrome b559. PS II membranes were prepared from spinach chloroplasts according to the method of Berthold et al. (1981) with the modifications of Ford and Evans (1983) and were stored at −80 °C until use. Cyt *b*559 was purified from PS II membranes using the procedure of Metz et al. (1983) with the following modifications. The DEAE-Sephadex column was replaced by a DEAE-Sephacel column and the Cyt *b*559 was eluted with 50 mM Tris-HCl, pH 8.0, 2 mM dithiothreitol, 0.05% Triton X-100 (w/v), and 250 mM KCl. Removal of the majority of the detergent and concentration of the sample were done using a Centricon-10 ultrafiltration cell (Amicon) and successive washing steps with 250 mM KCl, 5 mM Tris-HCl, pH 8.0, and 5 mM $MgCl_2$ in H_2O or with 250 mM KCl, 5 mM Tris-DCl, pD 8.0, and 5 mM $MgCl_2$ in D_2O. Purified and concentrated Cyt *b*559 was stored at −30 °C until use.

In some cases, a further concentration step was done by centrifugation in a speed vacuum concentrator to reach 0.5–1 mM (as estimated by the absorption at 559 nm). Studies at different pH were done using Tris-HCl buffer, pH 8 or 9, or Mes-NaOH buffer, pH 5 or 6.4. Controls of the sample contamination by cytochromes b_6 and f were done by EPR and found to be less than 2% after double integration of the g_z peaks and use of the semiempirical relation between g_z peak area and spin concentration (De Vries & Albracht, 1979).

Electrochemistry. The electrochemical cell is described in Moss et al. (1990). It has a path length below 10 μm. A 6-μm gold minigrid was used as the working electrode, placed on a calcium fluoride window. The 15-μL sample was deposited on the electrode and covered by a second window. An Ag/AgCl/3 M KCl system was used as the reference electrode. All the potentials are quoted versus SHE; we add 208 mV for the potentials recorded with a Ag/AgCl/3 M KCl reference electrode and 245 mV to the potentials reported in the literature and recorded with a SCE. For the model compounds dissolved in micelles of detergent, direct electrochemistry at the gold electrode was rapid and reversible and allowed acquisition of FTIR difference spectra with a high signal-to-noise ratio. The potential applied for reduction was −340 mV, and for reoxidation, +310 mV.

For the isolated Cyt *b*559, direct electrochemistry at the gold surface resulted in a poisoning of the electrode by adsorbed protein. Coating of the gold grid with a monolayer of pyridine-4-carboxaldehyde thiosemicarbazone (PATs-4) as a modifier was done according to the method of Frew and Hill (1988) to prevent aggregation and subsequent degradation of the protein at the electrode. PATs-4 adsorbs irreversibly to the gold electrode. The gold grid was incubated for 2 min in a 5 mM PATs-4 solution at 80 °C and subsequently washed several times with distilled water. Ferricyanide and neutral red were added as redox mediators to increase the speed of the electron exchange. The electrochemistry of the solution medium without Cyt *b*559 (or without hemin for the model compound studies) was performed to control the absence of any detectable contribution from the medium and the mediators to the electrochemically induced FTIR difference spectra (data not shown). Linear sweep voltammetry at different speeds was performed using an EG&G potentiostat interfaced to a computer as described in Mäntele et al. (1990). The potentiostat was triggered by a TTL output of the Bruker IFS 88 spectrometer for FTIR and FT-visible recordings.

Spectroscopy. FTIR and FT-visible spectra were taken on the same sample in the same conditions, on Bruker IFS 88 or Nicolet 60 SX spectrometers equipped with globar and tungsten sources, KBr and quartz beam splitters, and MCT-A and Si diode detectors. Acquisition of the difference spectra was done by averaging spectra from 10 (model compound) to 40 (Cyt *b*559) electrochemical cycles. Electrochemical experiments were carried out at room temperature. EPR spectra were recorded at 15 K in nonsaturating conditions with a Bruker ER 200D X-band spectrometer equipped with an Oxford Instruments cryostat, a HP5350B microwave frequency counter, and a Bruker ER035M NMR gaussmeter for the determination of g values.

Photooxidation of Cyt b559 was performed in PS II-enriched membranes resuspended in buffer A: 20 mM Mes, pH 6.4, 10 mM NaCl, 5 mM $MgCl_2$, and 10 mM $CaCl_2$. All the Cyt *b*559 was in the high-potential form (Cyt *b*559 HP). Sodium ascorbate (10 mM) was added to the sample to have 100% of Cyt *b*559 HP reduced before the experiment. To convert Cyt *b*559 to the LP form, PS II membranes were Tris-washed (in room light at 0 °C, 30 min, in a 0.8 M Tris buffer, pH 8.5) and then resuspended in buffer A with 30 mM sodium ascorbate to reduce Cyt *b*559 LP before the light-induced photooxidation experiments. When Cyt *b*559 LP is oxidized prior to freezing of the sample, a further illumination at 77 K results in the oxidation of a chlorophyll species (Visser & Rijgesberg, 1975). In order to photooxidize this Chl species instead of Cyt *b*559, the Tris-treated samples were incubated in buffer A with 5 mM ferricyanide. The preparation of the sample for FTIR measurements is described in Berthomieu et al. (1990). Difference spectra Cyt $b559_{ox}$ Q_A^-/Cyt $b559_{red}$ Q_A or Chl^+ Q_A^-/Chl Q_A were obtained between the dark-adapted state and after illumination at 60 K for 10 s with a tungsten lamp (150 W) equipped with red- ($\lambda > 645$ nm) and heat-absorbing filters. The Nicolet 60 SX and Bruker IFS 88 FTIR spectrometers are equipped with nitrogen- or helium-cooled cryostats. For EPR control experiments, illumination of PS II membranes at 77 K was done in EPR tubes using a nonsilvered dewar, filled with liquid nitrogen, with an 800-W projector through water- and heat-absorbing filters.

RESULTS

(*1*) *EPR Spectroscopy.* The model compounds, the isolated Cyt *b*559, and Cyt *b*559 in PS II membranes analyzed in the present study were controlled by EPR spectroscopy. All the g values and the relevant parameters [reviewed in Palmer (1985)] are presented in Table I and are compared to data from the literature.

(*a*) *Model Compounds and Isolated Cyt b559.* The FePP-(4-MeIm)$_2$ complex exhibited EPR signals with $g_z = 2.92$, $g_y = 2.26$, and $g_x = 1.57$, characteristic of a low-spin hexacoordinated form (Palmer, 1985; Walker et al., 1986). The g values are comparable for the FePP(Im)$_2$ and the FePP(1-MeIm)$_2$ complexes as presented in Table I. In contrast, at pH 12, where the effect of the two axial ligands deprotonation was studied for FePP(4-MeIm)$_2$, the EPR data show $g_z = 2.69$, $g_y = 2.25$, and $g_x = 1.79$. All the models studied here exhibited EPR spectra free from signals at $g = 6$, 4.3, and 2, indicating the absence of heme iron in the high-spin state, rhombic iron, and free radicals, respectively (Babcock et al., 1985; Palmer, 1985).

After isolation and purification, Cyt *b*559 exhibited EPR signals with $g_z = 2.92$, $g_y = 2.26$, and $g_x \approx 1.54$ at pH 8 (see Table I) in agreement with the values obtained by Babcock et al. (1985). Only very small signals were detected at $g = 6$, 4.3, and 2. Purified Cyt *b*559 was also studied at pH 5.0, 6.4, and 9.0 (see below). To test the stability of the samples under these conditions, they were incubated for 24 h at room temperature at the various pH. The EPR spectra were then recorded. No change in the g values was observed and no signals appeared at $g = 6$, 4.3, and 2.0, which indicates that no degradation of the cytochrome has occurred.

(*b*) *Cyt b559 in PS II Membranes.* In PS II membranes, two sets of g values (Table I) are found depending on the temperature at which Cyt *b*559 HP or LP is oxidized (Thompson et al., 1989). After photooxidation at low temperature, the g_z value is always higher than in a chemically oxidized or photooxidized Cyt *b*559 at room temperature or than in membranes annealed after low-temperature illumination (relaxed form). In our intact oxygen-evolving PS II membranes, only a small fraction of Cyt *b*559 was found oxidized with a g_z value equal to 3.03, characteristic of a room-temperature oxidized Cyt *b*559 HP. Illumination of this sample at 77 K resulted in the stable reduction of the plastoquinone Q_A and photooxidation of Cyt *b*559 HP (Knaff

Table I: EPR Parameters of Model Compounds, Purified Cyt *b*559, and Cyt *b*559 in PS II Membranes

	g_z	g_y	g_x	V/λ	Δ/λ	V/Δ	Σg_i^2	Φ[a]
Model Compounds								
Fe(III)PP-$(Im)_2$	2.96	2.24	1.51	1.84	3.43	0.54	16.1	20–25
Fe(III)PP-[4(5),MeIm]$_2$, pH 8	2.92	2.26	1.57	1.98	3.55	0.56	16.1	20–25
Fe(III)PP-$(1N\text{-MeIm})_2$	2.95	2.25	1.52	1.87	3.40	0.55	16.1	20–25
Fe(III)PP-[4(5),MeIm]$_2$, pH 12	2.69	2.25	1.79	2.86	4.78	0.60	15.5	20
Purified Cytochrome *b*559								
pH 5.0[b]	2.92	2.27	1.55	1.96	3.38	0.58	16.1	20–25
pH 8.0	2.92	2.26	1.54	1.93	3.39	0.57	16.0	20–25
pH 9.0[b]	2.91	2.27	1.55	1.97	3.36	0.59	16.0	20–25
Cytochrome *b*559 in PS II								
HP[c]	3.08	2.16	1.41	1.57	3.56	0.44	16.1	45–50
HP[c]	3.08[e]	2.16[e]	1.36[e,f]	1.51	3.35	0.45		45–50
HP[d,g]	3.03	2.19	1.44	1.65	3.49	0.47	16.0	45–50
HP[d]	3.05[e]	2.18[e]	1.40[e,f]	1.58	3.36	0.47		45–50
IP[c]	3.04[e]	2.17[e]	1.43[e,f]	1.62	3.58	0.45		45–50
IP[d]	3.01[e]	2.19[e]	1.46[e,f]	1.70	3.58	0.47		45–50
LP[c]	3.05	2.18	1.46	1.65	3.69	0.45	16.2	45–50
LP[d]	2.95	2.25	1.49	1.82	3.23	0.56	16.0	20–25
LP[d]	2.94[h]	2.26[h]	1.50[f,h]	1.86	3.23	0.58		20–25

[a] Deduced from the plot $V/\Delta = f(\Phi)$ in Quinn et al. (1987); Φ represents the angle between the plane of the imidazoles and the N1–N3 direction of the porphyrin. [b] Measured after incubation at room temperature for 24 h. [c] Nonrelaxed. [d] Relaxed. [e] Thompson et al. (1989). [f] Calculated according to the relation $g_z^2 + g_y^2 + g_x^2 = 16.0$. [g] Measured after annealing of a sample previously illuminated at 77 K. The g values from different batches of PS-II preparation might vary by about ±0.01 for g_z and g_y and ±0.02 for g_x. These variations did not affect the V/Δ values. No significant variation in g values was found with model compounds and purified Cyt *b*559. [h] Malkin and Vänngard (1980).

& Arnon, 1969) with a g_z value equal to 3.08 and characteristic of the nonrelaxed oxidized Cyt *b*559 HP. An intermediate form (Cyt *b*559 IP) has been reported (Thompson et al., 1989) with $E_m \approx 240$ mV. The absence of Cyt *b*559 IP characteristic g values (Table I) in the EPR spectra indicates that our preparations were free from this IP form (data not shown). In the Tris-treated PS II membranes, all the Cyt *b*559 was oxidized and exhibited an EPR signal at $g_z = 2.95$, characteristic of Cyt *b*559 LP (Malkin & Vänngard, 1980). Incubation of these samples in buffer A with 30 mM sodium ascorbate led to the reduction of Cyt *b*559 LP. Illumination at 77 K of these samples led to the stable photooxidation of Cyt *b*559 LP and photoreduction of Q_A. As with the Cyt *b*559 HP and IP (Thompson et al., 1989), we show that the LP form possesses two sets of g values depending on the temperature of the oxidation (see Table I). The respective amounts of photooxidized Cyt *b*559 HP or LP and Chl in the conditions used for FTIR spectroscopy were estimated by recording the EPR spectrum of samples after illumination at 77 K. Photooxidation of Cyt *b*559 HP or LP occurred in more than 85% of the PS II RCs.

According to Blumberg and Peisach (1971) [see also Palmer (1985) and Walker et al. (1984, 1986)], the six-coordinated low-spin heme irons can be characterized by three parameters: Δ/λ and V/λ represent the tetragonal and rhombic splitting parameters, respectively, and the rhombicity, V/Δ, is related to the structure of the heme–imidazole complexes. The parameters V/Δ, Δ/λ, and V/λ, calculated from the EPR g values, are also presented in Table I. The rhombicity parameters found for our model compounds are close to values reported in the literature (Babcock et al., 1985; Walker et al., 1986). The purified Cyt *b*559 as well as Cyt *b*559 LP oxidized at room temperature have V/Δ values similar to that found for heme–imidazole model compounds, whereas nonrelaxed Cyt *b*559 LP and relaxed and nonrelaxed Cyt *b*559 HP possess identical V/Δ parameters that differ significantly from those of model compounds and relaxed Cyt *b*559 LP.

(2) IR Oxidation Markers of the Hemin–Imidazole Complexes. Linear sweep voltammetry performed on the FePP(4-MeIm)$_2$ and FePP(Im)$_2$ complexes shows that the electrochemical reaction is a one-electron process with a high reversibility. This reversibility allows the averaging of several electrochemical cycles for the acquisition of FTIR and FT-visible difference spectra.

As an example, the cyclic voltammogram for FePP(4-MeIm)$_2$ is displayed in the inset of Figure 1. The midpoint potential, measured as the average of the anodic and cathodic peak potentials, is observed at −72 mV (versus SHE) for FePP-(4-MeIm)$_2$ and at −2 mV for FePP(Im)$_2$ (not shown). Values of midpoint potentials for the Fe^{III}/Fe^{II} couple have been observed in this range for 4-MeIm, Im, and 1-MeIm complexes of iron tetraphenylporphyrin (FeTPP) in the presence of an excess of ligand at −35, ≈−5, and 195 mV, respectively, by cyclic voltammetry in CH_2Cl_2 (Quinn et al., 1984). More than 90% of the complexes were reduced in less than 2 min after application of a potential of −340 mV, and the oxidation observed with an applied potential of +310 mV was even faster. The midpoint potential was observed upon deprotonation of the two axial ligands [for FeTTP(4-MeIm)$_2^{2-}$] at −505 mV (Quinn et al., 1983). We observe also a large effect of ligand deprotonation on FePP(4-MeIm)$_2$ with a midpoint potential at around −200 mV for the experiments done at pH 12 (not shown).

The visible absorption spectra of the electrochemically reduced and oxidized forms of the FePP(Im)$_2$ complex displayed in Figure 1A, as well as the spectral changes at 560, 530, and 434 nm in the reduced-minus-oxidized difference spectrum in Figure 1B, are in agreement with data reported in the literature for chemically reduced complexes (Babcock et al., 1985; Desbois et al., 1989). Furthermore, the symmetry of the electrochemically induced difference spectra demonstrates the good reversibility of the method.

The IR absorption spectrum of the solution within the electrochemical cell for the FePP(4-MeIm)$_2$ complex (see Experimental Procedures) is displayed in Figure 2a. Its comparison with the IR absorption of a saturated solution of 4-MeIm (in H_2O at pH 8; Figure 2b) shows that, besides the H_2O band at ≈1640 cm^{-1}, only the IR modes of 4-MeIm can be seen in Figure 2a. Figure 2 also shows the FTIR absorption spectra of 4-MeIm in D_2O (c), of pure 1-MeIm (d), and of Im (e) and ^{15}NIm (f) in H_2O. Besides modes appearing in the δCH or ring stretching region (1400–1500 cm^{-1}) (Boinnard

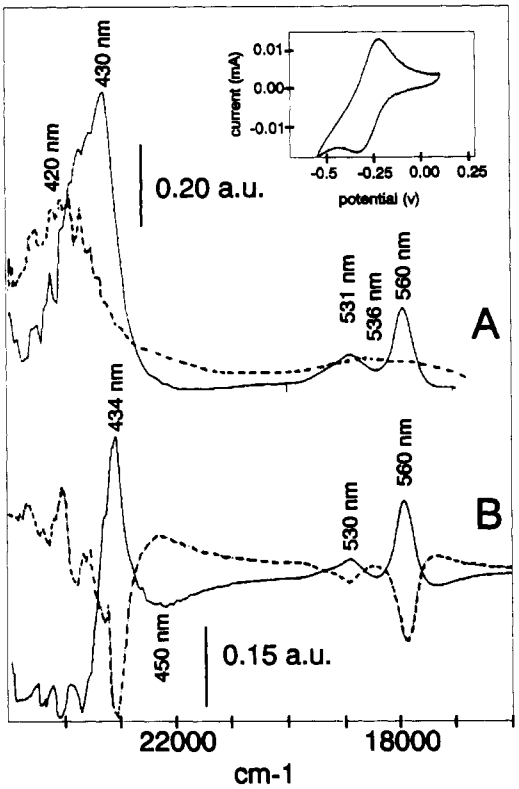

FIGURE 1: (A) Absorption spectra of the electrochemically oxidized (continuous line) and reduced (dashed line) forms of the $FePP(Im)_2$ complex in H_2O. FT-vis spectra were recorded with 256 coadded interferograms. a.u., absorbance unit. (B) Electrochemically induced oxidized-minus-reduced (thick line) and reverse (thin line) FTIR difference spectra obtained with $FePP(Im)_2$. Oxidative potential of 310 mV, reductive potential of −340 mV, 2560 coadded interferograms. (Inset) Cyclic voltammogram for the $FePP(4\text{-MeIm})_2$ complex. Scan speed: 2 mV/s (ref potential Ag/AgCl 3 M KCl).

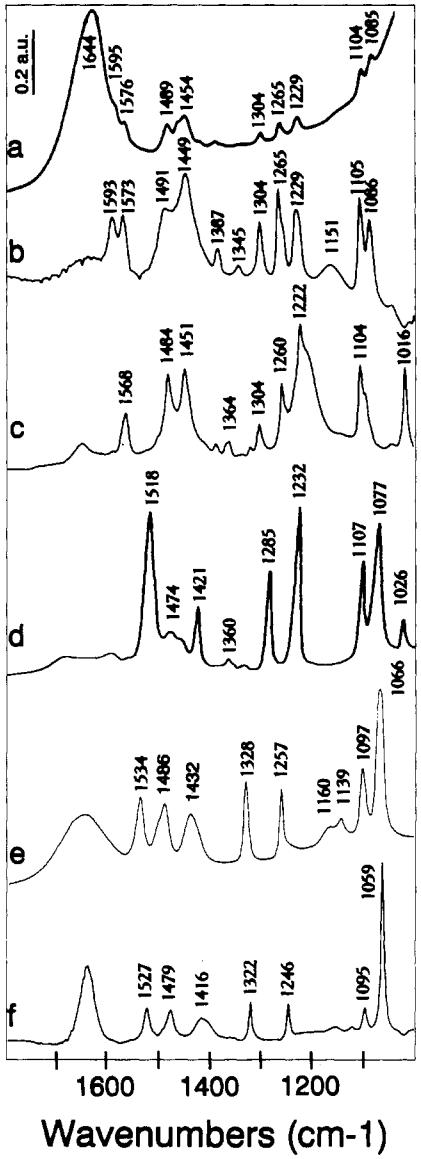

FIGURE 2: (a) FTIR absorption spectrum of the solution (pH 8.0) within the electrochemical cell for $FePP(4\text{-MeIm})_2$. Absorption spectra of (b) 4-MeIm in H_2O, (c) 4-MeIm in D_2O, (d) pure 1-MeIm, (e) Im in H_2O, and (f) ^{15}NIm in H_2O are shown. The band around 1644 cm^{-1} due to water absorption as well as the absorbance unit (a.u.) scale are only indicated for spectrum a; 128 coadded interferograms/spectrum.

et al., 1990; Cordes & Walter, 1968), the absorption of 4-MeIm is characterized by major bands at 1593, 1573, 1304, 1265, and 1229 cm^{-1}, whereas 1-MeIm displays strong modes at 1518, 1285, and 1232 cm^{-1}. The two modes observed at 1328 and 1257 cm^{-1} for Im are downshifted to 1322 and 1246 cm^{-1} upon $^{15}N/^{14}N$ substitution, in agreement with their attribution to δNH modes [at 1263 cm^{-1} in Cordes and Walter (1968)]. An overall downshift was observed upon $^{15}N/^{14}N$ substitution. Im, 1-MeIm, and 4-MeIm display two specific vibration modes around 1060–1090 or 1100 cm^{-1}. For Im, two modes observed at 1097 (almost insensitive to $^{14}N/^{15}N$ exchange) and 1066 cm^{-1} correspond to signals reported at 1099 and 1057 cm^{-1} by Cordes and Walter (1968) and assigned to δCH and νCC and to δCH and to δNH, respectively. The absorption spectra will be used for the assignment of ligand modes in the FTIR difference spectra obtained by electrochemistry of the complexes.

IR modes sensitive to the oxidation state of the complexes are revealed in the electrochemically induced oxidized-minus-reduced (and reverse) difference spectra displayed in Figure 3. Contributions from both the heme and the ligands are expected in these spectra. Figure 3a shows the oxidized-minus-reduced (thick line) and reverse (thin line) FTIR difference spectra of the $FePP(4\text{-MeIm})_2$ complex in H_2O at pH 8. In the former spectrum, negative bands are characteristic of $Fe^{II}PP(4\text{-MeIm})_2$, positive ones of $Fe^{III}PP(4\text{-MeIm})_2$. The most prominent features are observed at 1553, 1535, and 1240 cm^{-1} for the reduced form and at 1571 and 1103 cm^{-1} for the oxidized one. Small negative signals are observed at 1613, 1595, 1455, 1415, 1337, and 1227 cm^{-1}, and positive ones are observed at 1603, 1499, 1478, and 1148 cm^{-1}. In addition a smaller negative contribution is consistently observed at 1626 cm^{-1}. The effects of H/D exchange (Figure 3b), pH (Figure 3c), and 4-MeIm replacement by 1-MeIm (Figure 3d), Im (Figure 3e), and ^{15}NIm (Figure 3f) have been investigated for band assignments.

The majority of the bands observed in Figure 3a are not affected by the H/D exchange, as shown in Figure 3b. However, a small signal at 1595/1603 cm^{-1} in H_2O disappears in D_2O. In addition, for the reduced form, the band at 1227 cm^{-1} is downshifted to 1217 cm^{-1} in D_2O, and for the oxidized form, the 1499-cm^{-1} signal is downshifted to 1495 cm^{-1}, while the major band at 1571 cm^{-1} is upshifted to 1580 cm^{-1}. This latter upshift could be related to the disappearance of the 1595/1603-cm^{-1} signal observed in Figure 3a for $FePP(4\text{-MeIm})_2$ in H_2O. In the absorption spectrum of 4-MeIm in H_2O (Figure 2b), a mode is also observed at 1593 cm^{-1}. This mode is absent for 4-MeIm in D_2O in Figure 2c (possibly downshifted to 1568 cm^{-1}). This supports the assignment of

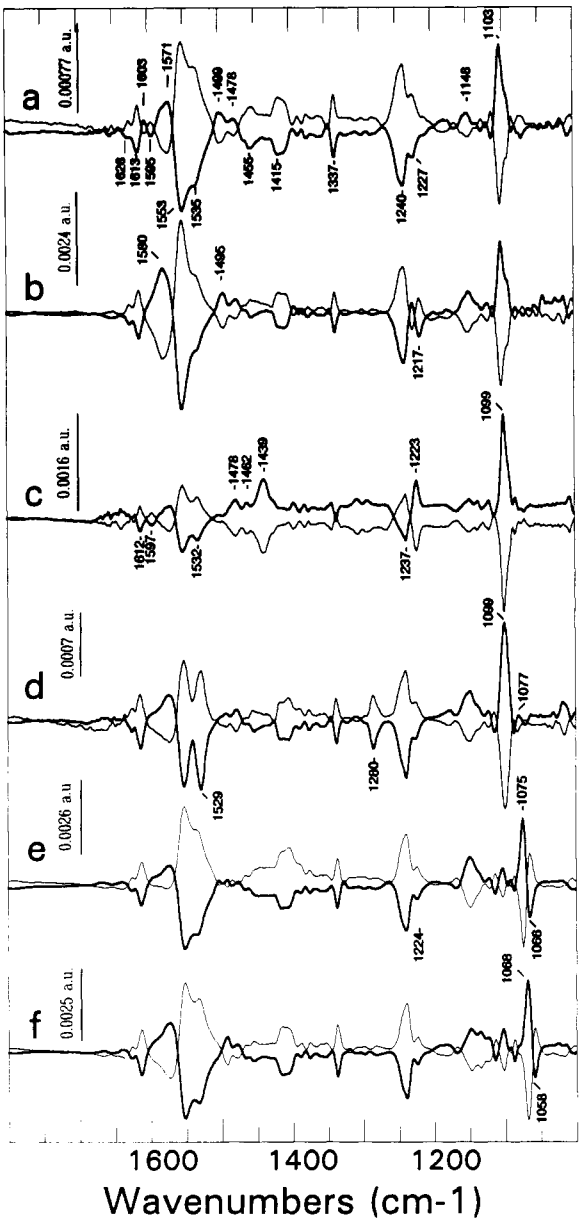

FIGURE 3: Electrochemically induced oxidized-minus-reduced (thick line) and reduced-minus-oxidized (thin line) FTIR difference spectra for (a) FePP(4-MeIm)$_2$ in H_2O at pH 8, (b) FePP(4-MeIm)$_2$ in D_2O at pD 8, (c) FePP(4-MeIm)$_2$ in H_2O at pH 12, (d) FePP(1-MeIm)$_2$ in H_2O, pH 8, (e) FePP(Im)$_2$ in H_2O, pH 8, and (f) FePP(^{15}NIm)$_2$ in H_2O, pH 8. Resolution, 4 cm^{-1}; ≈1280 coadded interferograms/spectrum. a.u., absorbance unit.

the differential signal observed at 1595/1603 cm^{-1} in Figure 3a to a 4-MeIm mode sensitive to the oxidation state of the iron.

The insensitivity of the 1553–1535-cm^{-1} modes to deuteration is in agreement with their assignment to porphyrin contributions. Comparison of FTIR difference spectra obtained with 4-MeIm, 1-MeIm, Im, and ^{15}NIm allows discrimination between skeletal or vinyl porphyrin modes, heme core size markers (influenced by the nature of the ligand), and ligand modes. The prominent signals at 1571/1553, 1535, 1240, and 1103 cm^{-1} in Figure 3a are also present in Figure 3, panels d and e, although the latter band is shifted to 1099 cm^{-1} for 1-MeIm and 1075 cm^{-1} for Im and the shoulder at 1535 cm^{-1} appears as a peak at 1529 cm^{-1} for 1-MeIm. The signals at 1571/1553 and 1240 cm^{-1}, which are not affected by the nature of the ligand, are thus assigned to heme skeletal modes. A number of smaller bands at 1626, 1613, 1478, 1455, 1415–1405, 1337, and 1148 cm^{-1}, which appear at the same frequency in Figure 3, panels a, d, and e, are also assigned to heme skeletal or vinyl modes (Table II). The extinction coefficient of the 1553-cm^{-1} heme mode was calculated for the different model compounds and found at 360 ± 20 M^{-1} cm^{-1}.

The assignment of the 1535-cm^{-1} signal (in Figure 3, panels a, b, and e) to a heme mode on the basis of its insensitivity to H/D exchange is reinforced by its lack of sensitivity to ^{14}N/^{15}N substitution on the Im ligand (Figure 3f). The lower frequency of this signal—observed at 1529 cm^{-1}—for the FePP(1-MeIm)$_2$ complex (Figure 3d) could be correlated to the impossibility for 1-MeIm to form a hydrogen bond, in contrast to 4-MeIm or Im. The variation of the frequency observed for the main positive band between 1103 and 1075 cm^{-1} in Figure 3 can be correlated to the different frequencies and amplitudes of two bands present in the IR spectra of the ligands, at 1105 and 1086 cm^{-1} for 4-MeIm, 1107 and 1077 cm^{-1} for pure 1-MeIm, and 1097 and 1066 cm^{-1} for Im (Figure 2, panels b, d, and e). For FePP(4-MeIm)$_2$ and FePP(1-MeIm)$_2$, the structured negative signal observed at 1103–1099 cm^{-1} (Figure 3) could result from the sensitivity of both modes of the ligand displayed in the 1103–1075-cm^{-1} region (Figure 2) to the redox state of the heme iron. The differential signal observed at 1075/1066 cm^{-1} for FePP(Im)$_2$ is attributed to a downshift upon reduction of the Im mode observed at 1066 cm^{-1} in Figure 2e. Furthermore, this differential signal is observed at 1068/1058 cm^{-1} for FePP(^{15}NIm)$_2$, in agreement with the downshift observed for the strongest 1066-cm^{-1} mode of Im in Figure 2e to 1059 cm^{-1} for ^{15}NIm in Figure 2f. Its assignment to a redox-sensitive ligand ring mode is thus demonstrated by the effect of Im ^{15}N labeling on FePP(Im)$_2$. This mode can constitute a marker sensitive to the nature of the heme ligands in cytochromes. A mode at 1280 cm^{-1} observed only in Figure 3d, which is also present at 1285 cm^{-1} in the absorption spectrum of pure 1-MeIm (Figure 2d) is assigned to a contribution from the ligand 1-MeIm. The comparison between the electrochemically induced difference spectra obtained with FePP(^{15}NIm)$_2$ and FePP(NIm)$_2$ demonstrates that, apart from the main ligand contribution at ≈1100 cm^{-1}, the difference spectra of Figure 3 are dominated by porphyrin modes.

The most striking feature of the electrochemically induced spectra of FePP(4-MeIm)$_2$ obtained at pH 12 (Figure 3c) is the size of the band at 1099 cm^{-1} (ligand mode), twice as large as the band at 1553 cm^{-1}. Other significant differences are observed at 1223, 1462, and 1439 cm^{-1}, the latter signal being probably a ligand mode observed at 1440 cm^{-1} at pH 12 (data not shown). While signals at 1571/1553, 1478, 1337, and 1148 cm^{-1} are unchanged at pH 12, the 1613-, 1595-, 1535-, 1240-, and 1103-cm^{-1} signals observed at pH 8 appear slightly shifted to 1612, 1597, 1532, 1237, and 1099 cm^{-1}, respectively.

Protonated Im or 4-MeIm are characterized by the stretching vibrations of their NH groups, arising at ≈3400 cm^{-1}, if it is free from interactions, or as a broad absorption band with six major peaks at 2400–3200 cm^{-1} (Anderson et al., 1961; Perchard & Novak, 1968; Zimmermann, 1961), if it is hydrogen-bonded, for example, in concentrated solutions in CCl_4. We do not have access to the NH stretching region above 3100 cm^{-1}, since the water absorbs too strongly there. The spectrum of 4-MeIm at pH 8 shows the characteristic absorptions of hydrogen-bonded ν(NH) between 3100 and 2400 cm^{-1} (data not shown). In the electrochemically induced difference spectra, a positive signal observed at 2651 cm^{-1} for FePP(Im)$_2$ and downshifted to 2633 cm^{-1} upon ^{14}N/^{15}N

Table II: Tentative Assignments of Bands (cm^{-1}) Observed in Redox-Induced FTIR Difference Spectra of Model Compounds

FePP(4-MeIm)$_2$		FePP(1-MeIm)$_2$		FePP(Im)$_2$		FePP(^{15}NIm)$_2$		
red	ox	red	ox	red	ox	red	ox	tentative assignments
1626		1626		1626		1626		vinyl CαCβ
1613		1613		1613		1613		CαCβ vinyl
1595	1605							4-MeIm
1553	1571	1553	1571	1553	1573	1553	1573	ν37(CaCm) or ν38(CbCb)
1535		1529		1535		1535		ν38(CbCb)
	1478		1478		1478			ν39(CaCm)
1455		1455		1455		1455		ν39(CaCm) or ν40(CaCb)
1415		1415		1415		1415		ν41(CaN)
1405		1405		1405		1405		
1337		1337		1337		1337		ν41(CaN) or νs(=CH$_2$ vinyl)
	1280							1-MeIm
1240		1239		1239		1239		δ42(CmH)
1227		1225		1224		1224		
	1148		1148		1148		1148	vinyl mode
	1103		1099					4-MeIm or 1-MeIm
				1066	1075	1054	1068	Im or ^{15}NIm (δCH and δNH)

substitution, absent for the FePP(1-MeIm)$_2$ complex and observed at $\approx$2640 cm^{-1} for FePP(4-MeIm)$_2$ (data not shown), is assigned to contributions from the protonated NH group of the ligand. This signal is interpreted in terms of a change in the strength of the hydrogen bond formed by the ligand upon oxidoreduction. In the 3100–2400-cm^{-1} region, other differential signals are observed at 2876 cm^{-1} for the oxidized form and at 2920–2921 and 2850–2854 cm^{-1} for the reduced form (data not shown). These signals, observed for all the model compounds and unaltered by ligand substitution or Im labeling, appear at too low frequency to account for the νCmH or νCbH of the porphyrin (Li et al., 1990). They are tentatively assigned to the CH_2 stretching mode of the methylene group of heme propionates.

(*3*) *Electrochemically Induced FTIR Difference Spectroscopy of Isolated Cyt b559.* The oxidized-minus-reduced (thick line) and reduced-minus-oxidized (thin line) difference spectra in the visible range for Cyt *b*559 in H_2O at pH 8 are presented in Figure 4, inset 2. The oxidized-minus-reduced difference spectrum shows a positive band at 410 nm and negative ones at 429, 528, and 559 nm, in agreement with values reported in the literature (Babcock et al., 1985; Metz et al., 1983). Using a molar extinction coefficient of 17 500 M^{-1} cm^{-1} at 559 nm (Cramer et al., 1986), the concentration of cytochrome involved in the electrochemical oxidoreduction can be estimated at 0.7 ± 0.2 mM.

Figure 4 shows the electrochemically induced FTIR difference spectra obtained at pH 8 in H_2O (Figure 4a) and in D_2O (Figure 4b). The reduced Cyt *b*559 absorbs at 1545 cm^{-1}, a frequency close to the 1553–1535-cm^{-1} bands observed for the reduced model compounds and assigned to porphyrin modes. The modes observed at 1406, 1337, and 1239 cm^{-1} for the reduced Cyt *b*559 and at 1104 cm^{-1} for the oxidized Cyt *b*559 (Figure 4, inset 1) correspond to the four modes observed at 1415–1405, 1337, 1240, and 1103 cm^{-1} for the FePP(4-MeIm)$_2$ complex and assigned to heme modes and 4-MeIm, respectively. The main signals in Figure 4, panels a and b, are observed between 1600 and 1700 cm^{-1}. Positive signals at 1656, 1628, and 1608 cm^{-1} in the oxidized-minus-reduced spectrum characterize Cyt *b*559$_{ox}$, while signals at 1685, 1673, 1641, and 1620 cm^{-1} are characteristic of Cyt *b*559$_{red}$. It cannot be decided whether the changes observed in the 1600–1630-cm^{-1} region are due to contributions from amino acid side chains (νC=C or δNH_x modes) or to vinyl modes, since the latter modes have been observed between 1600 and 1630 cm^{-1} in the RR spectra of isolated Cyt *b*559 (Babcock et al., 1985) and possibly at 1613 and 1626 cm^{-1}

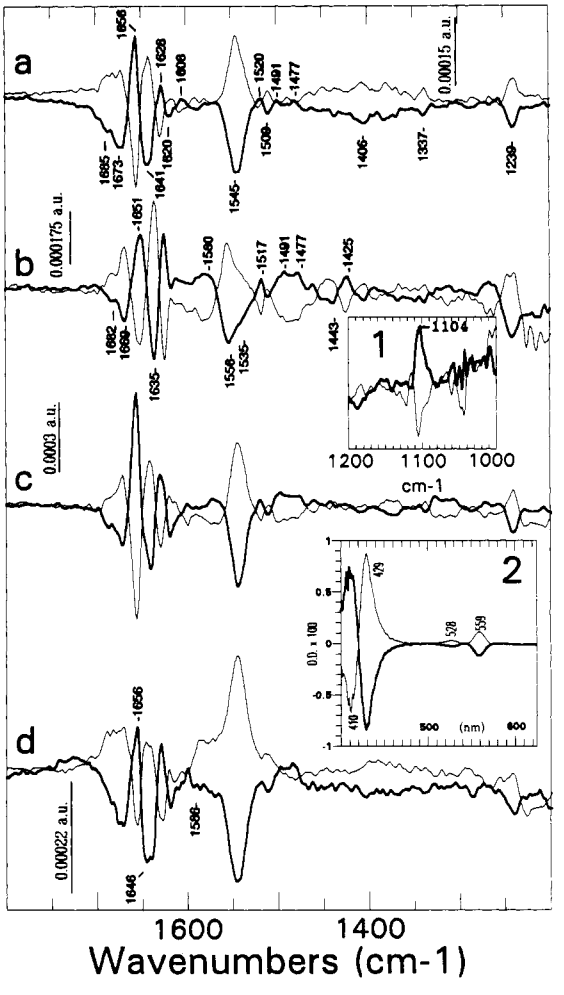

FIGURE 4: Electrochemically induced Cyt *b*559$_{ox}$-minus-Cyt *b*559$_{red}$ (thick line) and reverse (thin line) FTIR difference spectra (a) in H_2O at pH 8, (b) in D_2O, (c) in H_2O at pH 6.4, and (d) in H_2O at pH 5. Resolution, 4 cm^{-1}; $\approx$5120 coadded interferograms/spectrum. a.u., absorbance unit. (Inset 1) FTIR difference spectra in H_2O at pH 6.4, 1000–1200-cm^{-1} range. Amplitude of the signal is magnified by a factor equal to 1.5 in comparison with spectrum c. (Inset 2) Cyt *b*559$_{ox}$-minus-Cyt *b*559$_{red}$ (thick line) and reverse (thin line) difference spectra in H_2O at pH 8, in the visible range.

in the FTIR difference spectra of model compounds (see Discussion). The bands appearing above 1630 cm^{-1} are absent in the FTIR difference spectra obtained with FePP–imidazole complexes (Figure 3), demonstrating their belonging to the protein moiety. The absorption of peptide C=O stretching

Table III: Tentative Assignments of Bands (cm^{-1}) Observed in Redox-Induced FTIR Difference Spectra of Isolated and in Vivo Cyt *b*559

isolated Cyt *b*559				Cyt *b*559 HP		Cyt *b*559 LP		
H_2O		D_2O						
ox	red	ox	red	ox	red	ox	red	assignments
						1700		propionic COOH or Glu or Asp COOH
	1685		1682					propionic COOH
	1673		1669		1673		1673	arginine side chain
1656		1651		1660		1660		amide I (amide I′ D_2O)
	1641		1635		1652		1652	amide I (amide I′ D_2O)
1628		1625		1625		1625		
	1620							
							1616	
	1545	1580	1556					heme (+ amide II H_2O)
							1523	
1520	1509	1517	1509		1518			phenol ring vibration of tyrosine
	1491		1491					complex histidine–heme
	1477		1477					heme ν39(CaCm)
		1443						amide II′
1406								heme
1337		1337						heme
1239		1239						heme δCmH
	1104		1104					histidine ligand

modes (amide I) are expected between 1690 and 1630 cm^{-1} depending on the secondary structure (notably at 1660–1650 cm^{-1} for α-helical structures; Susi, 1969). The positive signal observed at 1656 cm^{-1} upon oxidation of Cyt *b*559 can be assigned to a change of the vibrational energy of hydrogen-bonded peptide C=O, but it cannot be decided whether the band is shifted to 1673 or to 1641 cm^{-1}. Contributions from the C=O mode of protonated heme propionic groups are usually found between 1740 and 1700 cm^{-1} (Bellamy, 1975). The propionic C=O mode is the strongest band observed at 1706 cm^{-1} in the absorption spectrum of hemin chloride powder and at 1700 cm^{-1} for hemin chloride dissolved in ethanol [data not shown; see also Choi et al. (1983)]. Signals at 1693 cm^{-1} in the oxidized-minus-reduced FTIR difference spectra of cyt *c* (Moss et al., 1990) and at 1688 cm^{-1} for *c*559 and *c*556 hemes of *Rhodopseudomonas viridis* cytochrome (Nabedryk et al., 1991) have been assigned to propionic group contributions. We cannot exclude that a propionic group accounts for the signal at 1685 cm^{-1} in Cyt $b559_{red}$/Cyt $b559_{ox}$. The ν(C=N) IR mode of arginine side chains has been reported at 1673 cm^{-1} (Venyaminov & Kalnin, 1990) and could also explain the signal observed for Cyt *b*559 at 1673 cm^{-1}, as the model proposed by Cramer et al. (1986) involves interactions between arginine side chains and the heme propionates.

The effects of H/D exchange were studied to clarify the 1700–1600-cm^{-1} region. The IR absorption spectrum of the sample in D_2O (data not shown) shows the amide I′ band at 1646 cm^{-1}, tyrosine C=C modes at 1510 cm^{-1}, and the amide II′ band (δN–D) at 1457 cm^{-1}. In the electrochemically induced difference spectra (Figure 4), the D_2O effect consists of a downshift of the major bands appearing between 1600 and 1700 cm^{-1}. The bands at 1685, 1673, 1656, and 1641 cm^{-1} are shifted to 1682, 1669, 1651, and 1635 cm^{-1}, respectively, in D_2O. Such a downshift of $\approx$5 cm^{-1} is quite in agreement with the D_2O effect expected on peptide C=O vibrations in α-helices. The negative signal observed at 1545 cm^{-1} upon oxidation in H_2O (Figure 4a) appears shifted to 1556 cm^{-1} in D_2O (Figure 4b). The effect expected on the amide II N–H in-plane bending mode is a downshift of $\approx$100 cm^{-1} (Susi, 1969). An interpretation would be to consider that distinct modes absorb at 1545 cm^{-1} in H_2O. Heme contributions insensitive to H/D exchange have been observed in the FTIR difference spectra of the model compounds at 1553 cm^{-1} with a shoulder at 1535 cm^{-1} (Figure 3). The signal at 1556 cm^{-1} in Figure 4b (D_2O) could reflect this heme contribution, whereas the broad signal around 1443 cm^{-1} only observed in D_2O could well correspond to the amide II′ absorption. The 1545-cm^{-1} signal observed in Figure 4a could thus reflect superimposed absorption of the heme and the protein. A clear positive signal appears at 1580 cm^{-1} in D_2O as for the FePP(4-MeIm)$_2$ complex upon H/D exchange (Figure 3b). Negative bands at 1406, 1337, and $\approx$1240 cm^{-1} are unchanged in Figure 4b, a behavior that reinforces their assignment to heme modes. Signals at 1491 and 1477 cm^{-1} in D_2O are greatly enhanced compared to the spectra obtained in H_2O (Figure 4a). They may correspond to signals observed at 1494 and 1478 cm^{-1} in the FTIR difference spectra obtained with model compounds.

The differential signal observed at 1520/1509 cm^{-1} in H_2O and at 1517/1509 cm^{-1} in D_2O in Cyt $b559_{red}$/Cyt $b559_{ox}$ and which is absent in FTIR difference spectra obtained with model compounds could be due to a contribution from a tyrosine residue (Bendit, 1967).

The influence of pH on the IR modes was studied in the pH 5–8 range where the isolated Cyt *b*559 is stable over 24 h at ambient temperature. Figure 4, panels a, c, and d, show the electrochemically induced spectra obtained at pH 8, 6.4, and 5. The spectrum at pH 5 presents a negative band at 1586 cm^{-1} upon oxidation and a smaller size for the 1656/1646-cm^{-1} signal as compared to the 1545-cm^{-1} band. A summary of these assignments is presented in Table III.

(4) Low-Temperature Photooxidation of Cyt b559 in PS II Membranes by Light-Induced FTIR Difference Spectroscopy. The light-induced FTIR difference spectra Cyt *b*559 HP_{ox} Q_A^-/Cyt *b*559 HP_{red} Q_A and Cyt *b*559 LP_{ox} Q_A^-/Cyt *b*559 LP_{red} Q_A obtained by photooxidation at 60 K are displayed in Figure 5, panels a and b, respectively. With Tris-treated samples resuspended in buffer A with 5 mM ferricyanide to ensure that 100% of Cyt *b*559 LP was oxidized, illumination at 60 K induced the photooxidation of a Chl species and the reduction of Q_A (as controlled by EPR). The Chl^+ Q_A^-/Chl Q_A FTIR difference spectrum is displayed in Figure 5c.

The signals observed at 1738, 1724/1720, 1673, 1643/1637, and 1562/1556 cm^{-1} and the positive band at 1479 cm^{-1} are the main conserved features in the spectra of Figure 5, panels a–c. These signals are assigned to the $Q_A \rightarrow Q_A^-$ transition at low temperature since they are also observed in the FTIR difference spectra corresponding solely to Q_A

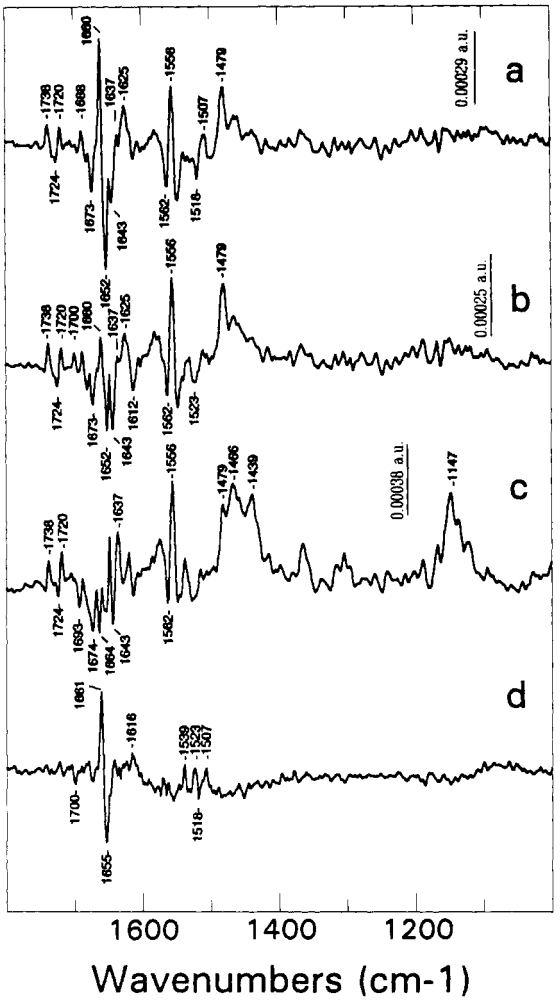

FIGURE 5: Light-induced FTIR difference spectra at 60 K corresponding to (a) Cyt *b*559 HP_{ox} Q_A^-/Cyt *b*559 HP_{red} Q_A, (b) Cyt *b*559 LP_{ox} Q_A^-/Cyt *b*559 LP_{red} Q_A, and (c) Chl^+ Q_A^-/Chl Q_A. (d) Double difference spectrum between spectra a and b optimized for the disappearance of Q_A^-/Q_A signals at 1724/1720, 1643, 1637, 1562/1556, and 1479 cm^{-1}; 1540 coadded interferograms. a.u., absorbance unit.

photoreduction in PS II at ambient temperature (Berthomieu et al., 1990; Noguchi et al., 1992). The signal observed in the amide II range at 1562/1556 cm^{-1} is found at 1559/1550 cm^{-1} at ambient temperature. Small differences in peak positions and widths of the bands preclude a meaningful interpretation of the double difference spectrum calculated between Cyt_{ox} Q_A^-/Cyt_{red} Q_A at 60 K and Q_A^-/Q_A at ambient temperature.

Assuming that the shape of the Q_A^-/Q_A spectrum is the same in Figure 5a–c, the differences observed between the spectra displayed in Figure 5 are interpreted as contributions of Cyt *b*559 HP or LP or Chl. Positive bands characteristic for Chl photooxidation are clearly observed at 1466, 1439, and 1147 cm^{-1} in Figure 5c. In the C=O absorption region, the spectrum results from the contributions of several overlapping modes and the interpretation is therefore not straightforward. Negative bands at 1693 and 1664 cm^{-1} observed only in the Chl^+ Q_A^-/Chl Q_A FTIR difference spectrum of Figure 5c could account for Chl modes altered by photooxidation. The νC=O mode of the 9-keto of isolated chlorophyll *a* has been reported at 1693 cm^{-1} in deuterated tetrahydrofuran and 1683 cm^{-1} in deuteromethanol and is sensitive to oxidation (Nabedryk et al., 1990; Tavitian et al., 1988). The signal observed at 1693 cm^{-1} is tentatively assigned to the Chl 9-keto group.

The Cyt *b*559 LP_{ox} Q_A^-/Cyt *b*559 LP_{red} Q_A difference spectrum (Figure 5b) shows overall similarity with Cyt *b*559 HP_{ox} Q_A^-/Cyt *b*559 HP_{red} Q_A (Figure 5a). We can rule out strong Chl contribution in these spectra, since the modes around 1450 and at 1147 cm^{-1}, characteristic of the Chl^+ state, are totally absent in Figure 5, panels a and b. Q_A^-/Q_A signals dominate the Cyt *b*559_{ox} Q_A^-/Cyt *b*559_{red} Q_A spectra. The differential signal at 1660/1652 cm^{-1} is the major IR change in Figure 5a and is not observed in Figure 5c. It is therefore the main characteristic of Cyt *b*559 HP photooxidation. This signal is also observed for Cyt *b*559 LP (Figure 5b), even if its intensity is at least 2 times smaller than for Cyt *b*559 HP, as compared to the 1479-cm^{-1} positive signal assigned to Q_A^-. A positive signal at 1625 cm^{-1} is conserved in the spectra of the HP and LP forms. Apart from the different intensity of the 1660/1652-cm^{-1} signal, the differences between the HP and LP forms of Cyt *b*559 are the small positive signal at 1700 cm^{-1} and the negative signals at 1612 and 1523 cm^{-1} for Cyt *b*559 LP and the negative signal at 1518 cm^{-1} for Cyt *b*559 HP. The differences between the mechanisms of photooxidation of Cyt *b*559 HP and LP are reflected in the double difference spectrum (Figure 5d) obtained by interactive subtraction of Figure 5, panels a and b, optimized by the disappearance of the features from Q_A^- and Q_A. The effect of H/D exchange on the light-induced Cyt *b*559 HP_{ox} Q_A^-/Cyt *b*559 HP_{red} Q_A spectrum obtained at 60 K consisted of the effects already reported for Q_A^-/Q_A (Berthomieu et al. 1990) as well as a downshift of the 1660/1652-cm^{-1} band to 1659/1650 cm^{-1} (data not shown).

DISCUSSION

Bisimidazole FePP complexes which provide good models of heme–histidine interactions in cytochromes and to some extent to hemoglobin and myoglobin (Spiro, 1983) have been extensively studied by RR spectroscopy. Information on IR active modes in these complexes are, however, very limited. In the present study, we combined electrochemistry and FTIR difference spectroscopy to describe IR markers of the oxidation state of several FePP–imidazole complexes in the 1800–1000-cm^{-1} range. Complexes of FePP with $(Im)_2$ and $(^{15}NIm)_2$ as well as $(1\text{-MeIm})_2$ and $(4\text{-MeIm})_2$ have been investigated to discriminate the modes of the ligands from those of the heme.

Kitagawa et al. (1978) have identified the in-plane skeletal RR modes and most of the IR skeletal vibrations of nickel octaethylporphyrin (NiOEP) and a normal coordinate analysis gave a reasonable assessment of the modes of this porphyrin with D_{4h} symmetry (Abe et al., 1978). In the 2000–1000-cm^{-1} range, nine IR-active modes were assigned to in-plane stretching contributions from all the bonds of the porphyrin ring (CbCb, CaCm, CaCb, and CaN) as well as to methine proton bending (Abe et al., 1978). From these studies, the IR contributions from the NiOEP, nickel protoporphyrin (NiPP) (Choi et al., 1982a; Spiro, 1983), and Fe^{III}PPCl (Choi et al., 1983) hemes have been assigned to ν37(CbCb) at 1604 cm^{-1} (NiOEP), ν38(CaCm) at 1566–1525 cm^{-1}, ν39(CaCm) at 1486–1458 cm^{-1}, ν40(CaCb) at 1440–1442 cm^{-1}, ν41(CaN) at 1386–1377 cm^{-1}, ν42(δCmH) at 1262–1280 cm^{-1}, and ν45(CaN) at 994–988 cm^{-1}. Recent normal mode analysis of nickel porphine gave values in the same range (Li et al., 1990) but with ν37 described as a ν(CaCm) mode at 1624 cm^{-1}, ν38 as a ν(CbCb) mode, and ν42(δCmH) found at 1150 cm^{-1}. Comparison of IR spectra of NiPP and NiOEP allowed the assignment of five additional IR modes of the vinyl groups at 1620 [ν(C=C)], 1343 [$\delta_s(CH_2)$], 1165 and 1118 [ν(CbCα)],

and 1089 cm^{-1} [$\delta_{as}(=CH_2)$] (Choi et al., 1982a; Spiro, 1983; Spiro & Strekas, 1974). No IR data concerning porphyrin–imidazole complexes are available in this frequency range. Nevertheless, comparison with RR data on these complexes (Choi et al., 1982a,b; Desbois & Lutz, 1992; Desbois et al., 1989; Spiro, 1983; Spiro et al., 1979) is useful insofar as in protoporphyrin derivatives, by virtue of their asymmetric position, the vinyl groups destroy the porphyrin symmetry center and can consequently induce Raman activity in typical IR modes and vice versa. For example, the IR-active ν37(CbCb) and ν38(CaCm) modes are observed at 1604 and 1560 cm^{-1} in RR spectra of $FePP(Im)_2$ (Desbois et al., 1989; Spiro, 1983).

Assignments of IR modes sensitive to the oxidation state of $FePP(Im)_2$ and $FePP(MIm)_2$ complexes are presented in Table II. The redox-sensitive signals at 1626, 1613, 1574/1553, 1535, 1478, 1455, 1415, 1337, 1240, and 1148 cm^{-1} can be assigned to heme modes. We tentatively assign the changes observed at 1574/1552 and 1535 cm^{-1} in Figure 3 to heme ν38(CbCb) and/or ν37(CaCm) modes (see above). The signals observed at 1478 (ox) and 1455 cm^{-1} (red) could also correspond to the ν39(CaCm) mode. The ν4(CaN) RR mode constitutes the most sensitive oxidation marker in RR spectra and appears at 1375–1360 cm^{-1}. There is no strong signal at 1380–1350 cm^{-1} in the electrochemically induced FTIR difference spectra that could correspond to this mode. This observation is consistent with the absence of this redox marker in the electrochemically oxidized cyt *c* (Moss et al., 1990) or in photochemically oxidized cyt of *Rps. viridis* (Nabedryk et al., 1991). The small signals observed at 1337 or 1415–1405 cm^{-1} in the FTIR difference spectra of Figure 3, however, could account for the ν41(CaN) IR mode [see above; this mode is assigned at 1319–1338 and 1331 cm^{-1} for nickel porphine and NiTPP by Li et al. (1990)]. Another possible assignment for the 1337-cm^{-1} mode is to a νs($=CH_2$ vinyl), as observed at 1343 cm^{-1} for NiPP (Choi et al., 1982a). The 1240-cm^{-1} mode could correspond to the δ42(CmH). The signals observed at 1626, 1613, and 1148 cm^{-1} upon reduction are tentatively assigned to vinyl contributions. The electrochemistry of a complex with mesoporphyrin would help clarify these assignments. Modes of ligands have also been characterized; essentially a marker of the nature of the ligand is found around 1100 cm^{-1} for the oxidized FePP complexes. The effect of imidazole ligand deprotonation on the RR frequencies of $FePP(Im)_2$ complexes has been studied by Desbois and Lutz (1992). These authors observed a downshift of 2–10 cm^{-1} on markers of the porphyrin core size (ν4, ν10, and ν11 modes) and on the ν38 mode. In Figure 3, panels a and c, a 3-cm^{-1} downshift is observed on the signal at 1535 cm^{-1} (to 1532 cm^{-1}), tentatively assigned to the ν38 mode, but the largest effects are observed on ligand modes at 1099 and 1439 cm^{-1}.

The study of the IR modes sensitive to the oxidation state of the $FePP(4\text{-}MeIm)_2$, $FePP(1\text{-}MeIm)_2$, and $FePP(Im)_2$ complexes allows the discrimination of heme and protein modes in the FTIR difference spectra obtained by electrochemistry of the isolated Cyt *b*559. In the electrochemically induced difference spectra of isolated Cyt *b*559, the signals at 1580/1556, 1535, 1406, 1337, and 1239 cm^{-1} can be assigned unambiguously to heme modes. The band at 1104 cm^{-1} (Figure 4, inset 1), very comparable to the 4-MeIm signal observed at 1103 cm^{-1} in the oxidized $FePP(4\text{-}MeIm)_2$ complex (Figure 3a), is assigned to the histidine ligands. Furthermore, the comparison of the amplitudes of the 1104- and 1556-cm^{-1} signals in the FTIR difference spectra of isolated Cyt *b*559 with the data obtained at pH 12 and 8 with the $FePP(4\text{-}MeIm)_2$ model compound seems to indicate that the histidine ligands would be protonated in isolated Cyt *b*559 at pH 8. The excellent agreement between model compounds and isolated Cyt *b*559 reinforces the validity of the model of a heme iron coordinated to two histidine residues in Cyt *b*559 (Cramer et al., 1986).

The participation of the protein moiety to the charge stabilization in the isolated Cyt *b*559 is demonstrated by the presence of IR signals between 1600 and 1700 cm^{-1} (Figure 4 and Table III) and their absence in the difference spectra obtained with the iron–protoporphyrin model compounds. We assign the signal observed at 1656/1641 cm^{-1} in Figure 4a to the absorption change of hydrogen-bonded peptide C=O group(s). Amino acid side chains of arginine and tyrosine could contribute to the difference spectra at 1673 and 1520/1509 cm^{-1}. A strong pH effect is observed between pH 6.4 and 5.

In situ, photooxidation of both Cyt *b*559 HP and LP is associated with a differential signal at 1660/1652 cm^{-1} that we propose to correspond to the 1656/1641-cm^{-1} signal observed in vitro. The differences in the temperature of the two experiments in vitro (ambient temperature) and in situ (60 K), the contribution of Q_A^-/Q_A in the photoinduced difference spectra, as well as a possible change in environment of the protein could explain the shift observed between the frequency of the amide I signal in vitro and in situ.[2] In the Cyt *b*559 LP_{ox} Q_A^-/Cyt *b*559 LP_{red} Q_A difference spectrum, the 1660/1652-cm^{-1} band amplitude is half of that observed in the photooxidation of Cyt *b*559 HP, as compared to the Q_A^- absorption at 1479 cm^{-1}. This could imply that the signal results from twice as many peptide C=O groups for Cyt *b*559 HP as for Cyt *b*559 LP. For isolated Cyt *b*559, the extinction coefficient of the 1656/1641-cm^{-1} differential signal was estimated at $\approx$970 M^{-1} cm^{-1} (by comparison with the heme mode at 1556 cm^{-1}). If we assume an extinction coefficient of 700 $\pm$ 100 M^{-1} cm^{-1} for the 1479-cm^{-1} signal of Q_A^- (Bauscher et al., 1990), we find that the amide I differential signal has a comparable amplitude in isolated Cyt *b*559 and in Cyt *b*559 LP.

X-ray data on several hemoproteins show that at least one histidine side chain axially bound to the heme iron is also generally hydrogen-bonded to an amide carbonyl or to an electronegative amino acid residue of the polypeptide chain (Mathews et al., 1972; Salemme et al., 1973; Takano & Dickerson, 1981). The signals observed at 1656/1641 cm^{-1} (isolated Cyt *b*559) or 1660/1652 cm^{-1} (in situ) in the FTIR difference spectra could result from the change of interaction between the imidazole NH group of the histidine and the peptide backbone, in the α-helices of polypeptides α and/or β. If we consider the symmetry of the model proposed by Cramer et al. (1986) as well as the sequence homology around the two histidine residues, we may speculate that one peptide C=O from each α-helix is involved in a hydrogen bond with the NH group of each histidine ligand in Cyt *b*559 HP, whereas for Cyt *b*559 LP, the interaction between one of the histidines and the backbone only would be conserved, the other histidine forming an interaction with an amino acid side chain instead of the backbone.

[2] With isolated Cyt *b*559, the FTIR difference spectra in Figure 4 correspond to the fully relaxed states. In contrast, with Cyt *b*559 in PS II membranes, low-temperature photooxidation results in generation of the nonrelaxed forms (Table I). Therefore, in the low-temperature spectra of Figure 5, some of the features characteristic of oxidized Cyt *b*559 may not be observed.

A useful tool to investigate structural changes in the heme–histidine ligands environment is EPR spectroscopy, since it is sensitive to the respective orientation of imidazole planes and heme. For heme–imidazole model compounds with parallel imidazole planes, on the basis of crystallographic data, Quinn et al. (1987) found a linear relationship between the rhombicity parameter (V/Δ) obtained from the EPR g values (see Results) and the angle Φ (dihedral angle between the N1–N3 porphinato vector and the imidazole planes). For Cyt *b*559, it was proposed that the axial ligands were parallel for Cyt *b*559 LP and perpendicular for Cyt *b*559 HP (Babcock et al., 1985). Nevertheless, the characteristic EPR signal with a strong g_{max} above 3.2 expected for heme–imidazole complexes with a large angle between the two imidazole planes (Walker et al., 1984, 1986) is not observed for Cyt *b*559 HP. If we assume that Cyt *b*559 possesses parallel axial ligands in both low- and high-potential forms, we may tentatively deduce from the V/Δ parameter the different angles Φ for the different forms Cyt *b*559 HP and LP. For Cyt *b*559 HP and LP photooxidized at 77 K, the value of Φ is around 45°, whereas the Φ value calculated for the relaxed Cyt *b*559 LP is ≈20–25° (see Table I) and is equivalent to the value found for both model compounds and isolated Cyt *b*559. The different V/Δ in Cyt *b*559 LP photooxidized at low temperature and after annealing indicates that the photoooxidation of this cytochrome is followed by a reorganization of the ligands, allowed at higher temperatures. In the Cyt *b*559 LP_{ox} Q_A^-/Cyt *b*559 LP_{red} Q_A FTIR difference spectrum, we observe the redox changes that will lead to a reorganization of the ligands around the heme in the oxidized form. The EPR data are quite in agreement with the IR data in the amide I range suggesting different environments or interactions of the histidine ligands in Cyt *b*559 HP and LP. The positive signal at 1700 cm^{-1} (Figure 5b), characteristic of Cyt *b*559 LP photooxidation, could arise from a protonated heme propionic group. The present FTIR data are consistent with a change in environment of one histidine ligand and a propionic group of the heme for Cyt *b*559 LP as compared to Cyt *b*559 HP, although it cannot be decided if a deprotonation of one of the histidine ligands occurs in Cyt *b*559 LP as postulated by Desbois and Lutz (1992). The differences observed in the FTIR spectra of Cyt *b*559 HP and LP demonstrate that the mechanisms of heme oxidation in situ imply different molecular processes for the two forms Cyt *b*559 HP and LP. These data seem to indicate that the environment of one histidine ligand is modified in Cyt *b*559 LP and could constitute an important factor regulating the midpoint potential of Cyt *b*559.

ACKNOWLEDGMENT

We acknowledge for very useful discussions J.-M. Ortega and A. Desbois, who also provided us a paper before publication, and W. A. Cramer for careful reading of the manuscript. We are grateful to Dr. Moss for help with the first electrochemical experiments.

REFERENCES

Abe, M., Kitagawa, T., & Kyogoku, Y. (1978) *J. Chem. Phys. 69*, 4526–4534.

Allen, J. P., Feher, G., Yeates, T. O., Komiya, H., & Rees, D. C. (1987) *Proc. Natl. Acad. Sci. U.S.A. 84*, 5730–5734.

Anderson, D. M. W., Duncan, J. L., & Rossotti, F. J. C. (1961) *J. Chem. Soc. 140*, 2165–2171.

Arnon, D. I., & Tang, G. (1988) *Proc. Natl. Acad. Sci. U.S.A. 85*, 9524–9528.

Babcock, G. T., Widger, W. R., Cramer, W. A., Oertling, W. A., & Metz, J. G. (1985) *Biochemistry 24*, 3638–3645.

Bauscher, M., Nabedryk, E., Bagley, K. A., Breton, J., & Mäntele, W. (1990) *FEBS Lett. 261*, 191–195.

Bellamy, L. J. (1975) *The Infrared Spectra of Complex Molecules* (Chapman & Hall, Eds.) 4th ed., Methuen, London.

Bendit, E. G. (1967) *Biopolymers 5*, 325–333.

Berthold, D. A., Babcock, G. T., & Yocum, C. F. (1981) *FEBS Lett. 61*, 231–234.

Berthomieu, C., Nabedryk, E., Mäntele, W., & Breton, J. (1990) *FEBS Lett. 269*, 363–367.

Blumberg, W. E., & Peisach, J. (1971) in *Bioinorganic Chemistry* (Dessy, R., Willard, J., & Taylor, L., Eds.) Advances in Chemistry Series, Vol. 100, pp 271–291, American Chemical Society, Washington, DC.

Boinnard, D., Cassoux, P., Petrouleas, V., Savariault, J.-M., & Tuchagues, J.-P. (1990) *Inorg. Chem. 29*, 4144–4122.

Braiman, M. S., & Rothschild, K. J. (1988) *Annu. Rev. Biophys. Biophys. Chem. 17*, 541–570.

Choi, S., Spiro, T. G., Langry, K. C., & Smith, K. M. (1982a) *J. Am. Chem. Soc. 104*, 4337–4344.

Choi, S., Spiro, T. G., Langry, K. C., Smith, K. M., Budd, D. L., & La Mar, G. N. (1982b) *J. Am. Chem. Soc. 104*, 4337–4344.

Choi, S., Lee, J. J., Wei, Y. H., & Spiro, T. G. (1983) *J. Am. Chem. Soc. 105*, 3692–3707.

Churg, A. K., & Warshel, A. (1986) *Biochemistry 25*, 1675–1681.

Cordes de N. D., M., & Walter C. S. C., (1968) *Spectrochim. Acta 24A*, 237–252.

Cramer, W. A., & Whitmarsh, J. (1977) *Annu. Rev. Plant Physiol. 28*, 133–172.

Cramer, W. A., Theg, S. M., & Widger, W. R. (1986) *Photosynth. Res. 10*, 393–403.

Deisenhofer, J., Epp., O., Miki, K., Huber, R., & Michel, H. (1985) *Nature 318*, 618–624.

Dekker, J. P., Bowbly, N. R., & Yocum, C. F. (1989) *FEBS Lett. 254*, 150–154.

dePaula, J. C., Innes, J. B., & Brudvig, G. W. (1985) *Biochemistry 24*, 8114–8120.

Desbois, A., & Lutz, M. (1992) *Eur. Biophys. J. 20*, 321–335.

Desbois, A., Tegoni, M., Gervais, M., & Lutz, M. (1989) *Biochemistry 28*, 8011–8022.

De Vries, S., & Albracht, S. P. J. (1979) *Biochim. Biophys. Acta 546*, 335–340.

El-Kabbani, O., Chang, C.-H., Tiede, D., Norris, J., & Schiffer, M. (1991) *Biochemistry 30*, 5361–5369.

Ford, R. C., & Evans, M. C. W. (1983) *FEBS Lett. 160*, 159–164.

Frew, J. E., & Hill, H. A. O. (1988) *Eur. J. Biochem. 172*, 261–269.

Gounaris, K., Chapman, D. J., & Barber, J. (1989) *Biochim. Biophys. Acta 973*, 296–301.

Gunner, M. R., & Honig, B. (1991) *Proc. Natl. Acad. Sci. U.S.A. 88*, 9151–9155.

Heber, U., Kirk, M., & Boardman, N. K. (1979) *Biochim. Biophys. Acta 546*, 292–306.

Herrmann, R. G., Alt, J., Schiller, B., Widger, W. R., & Cramer, W. A. (1984) *FEBS Lett. 176*, 239–244.

Kassner, R. J. (1972) *Proc. Natl. Acad. Sci. U.S.A. 69*, 2263–2267.

Kitagawa, T., Abe, M., & Ogoshi, H. (1978) *J. Chem. Phys. 69*, 4516–4525.

Klimov, V. V., Allakhverdier, S. I., Demeter, S., & Krasnovskii, A. A. (1980) *Dokl. Akad. Nauk. SSSR 249*, 227.

Knaff, D. B., & Arnon, D. I. (1969) *Proc. Natl. Acad. Sci. U.S.A. 63*, 956.

Lemberg, R., & Barrett, J. (1973) in *Cytochromes*, Academic Press, New York.

Li, X.-Y., Czermmszewicz, R. S., Kincaid, J. R., Su, Y. O., & Spiro, T. G. (1990) *J. Phys. Chem. 94*, 31–47.

Malkin, R., & Vänngard, T. (1980) *FEBS Lett. 111*, 228–231.

Mäntele, W., Leonhard, M., Bauscher, M., Nabedryk, E., Breton, J., & Moss, D. A. (1990) in *Reaction Centers of Photosynthetic Bacteria* (Michel-Beyerle, M. E., Ed.) Springer Series in Biophysics, Vol. 6, pp 31–44, Springer Verlag, Berlin.
Mathews, F. S., Levine, M., & Argos, P. (1972) *J. Mol. Biol. 64*, 440–464.
Metz, J. G., Ulmer, G., Bricker, T. M., & Miles, D. (1983) *Biochim. Biophys. Acta 725*, 203–209.
Moore, G. R., Harris, D. E., Leitch, F. A., & Pettigrew, G. W. (1984) *Biochim. Biophys. Acta 764*, 331–342.
Moss, D., Nabedryk, E., Breton, J., & Mäntele, W. (1990) *Eur. J. Biochem. 187*, 565–572.
Nabedryk, E., Leonhard, M., Mäntele, W., & Breton, J. (1990) *Biochemistry 29*, 3242–3247.
Nabedryk, E., Berthomieu, C., Verméglio, A., & Breton, J. (1991) *FEBS Lett. 293*, 53–58.
Namba, O., & Satoh, K. (1987) *Proc. Natl. Acad. Sci. U.S.A. 84*, 109–112.
Nogushi, T., Ono, T.-A., & Inoue, Y. (1992) *Biochemistry 31*, 5953–5956.
Ortega, J.-M., Hervas, M., & Losada, M. (1988) *Eur. J. Biochem. 171*, 449–455.
Palmer, G. (1985) *Biochem. Soc. Trans. 13*, 548–560.
Perchard, C., & Novak, A. (1968) *J. Chem. Phys. 48*, 3079–3084.
Quinn, R., Strouse, C. E., & Valentine, J. S. (1983) *Inorg. Chem. 22*, 3934–3940.
Quinn, R., Mercer-Smith, J., Burstyn, J. N., & Valentine, J. S. (1984) *J. Am. Chem. Soc. 106*, 4136–4144.
Quinn, R., Valentine, J. S., Byrn, M. P., & Strouse, C. E. (1987) *J. Am. Chem. Soc. 109*, 3301–3308.
Rich, P. R., & Bendall, D. S. (1980) *Biochim. Biophys. Acta 591*, 153–161.
Rutherford, A. W. (1985) *Biochim. Biophys. Acta 807*, 189–201.
Rutherford, A. W., Zimmermann, J.-L., & Bousac, A. (1992) in *The Photosystems: Structure, Function and Molecular Biology, Oxygen Evolution* (Barber, J., Ed.) pp 179–229, Elsevier Science Publishers, Amsterdam.
Salemme, F. R., Freer, S. T., Xuong, N. H., Alden, R. A., & Kraut, J. (1973) *J. Biol. Chem. 248*, 3910–3921.
Satoh, K., Hansson, O., & Mathis, P. (1990) *Biochim. Biophys. Acta 1016*, 121–126.
Spiro, T. G. (1983) in *Iron Porphyrins* (Lever, A. B. P., & Gray, H. B., Eds.) Physical and Bioinorganic Chemistry Series, Chapter 3, pp 89–159, Addison-Wesley Publishing Co., London.
Spiro, T. G., & Streakas, T. C. (1974) *J. Am. Chem. Soc. 96*, 338–345.
Spiro, T. G., Stong, J. D., & Stein, P. (1979) *J. Am. Chem. Soc. 101*, 2648–2655.
Susi, H. (1969) in *Structure and Stability of Biological Macromolecules* (Timasheff, S. N., & Fasman, G. D., Eds.) Vol. 2, pp 575–663, Dekker, New York.
Takano, T., & Dickerson, R. E. (1981) *J. Mol. Biol. 153*, 95–115.
Tavitian, B. A., Nabedryk, E., Wollenweber, A., Mäntele, W., & Breton, J. (1988) in *Spectroscopy of Biological Molecules—New Advances* (Schmid, E. D., Schneider, F. W., & Siebert, F., Eds.) pp 297–300, Wiley and Sons, Chichester, U.K.
Thompson, L. K., & Brudwig, G. W. (1988) *Biochemistry 27*, 6653–6658.
Thompson, L. K., Miller, A.-F., Buser, C. A., de Paula, J., & Brudvig, G. W. (1989) *Biochemistry 28*, 8048–8056.
Valentine, J. S., Sheridan, R. P., Allen, L. C., & Kahn, P. C. (1979) *Proc. Natl. Acad. Sci. U.S.A. 76*, 1009–1013.
Venyaminov, S. Yu., & Kalnin, N. N. (1990) *Biopolymers 30*, 1243–1257.
Verméglio, A., & Mathis, P. (1974) *Biochim. Biophys. Acta 368*, 9–17.
Verméglio, A., Breton, J., Barouch, Y., & Clayton, R. K. (1980) *Biochim. Biophys. Acta 593*, 299–311.
Visser, J. M. W., & Rijgersberg, C. P. (1975) *Proceedings of the Third International Congress on Photosynthesis* (Avron, M., Ed.) pp 399–408, Elsevier Science Publishers, Amsterdam.
Walker, F. A., Reis, D., & Balke, V. L. (1984) *J. Am. Chem. Soc. 106*, 6888–6898.
Walker, F.-A., Huynh, B. H., Scheidt, W. R., & Osvath, S. R. (1986) *J. Am. Chem. Soc. 108*, 5288–5297.
Westhoff, P., Alt, J., Widger, W. R., Cramer, W. A., & Herrman, R. G. (1985) *Plant Mol. Biol. 4*, 103–110.
Widger, W. R., Cramer, W. A., Hermodson, M., Meyer, D., & Gullifor, M. (1984) *J. Biol. Chem. 259*, 3870–3876.
Widger, W. R., Cramer, W. A., Hermodson, M., & Herrmann, R. G. (1985) *FEBS Lett. 191*, 186–190.
Zimmermann, H. (1961) *Z. Electrochem. 65*, 821–840.